Successively refined models for crack tip plasticity in polymer blends

Pijnenburg, KGW; Seelig, T; van der Giessen, E

Published in:
European Journal of Mechanics A-Solids

DOI:
10.1016/j.euromechsol.2005.04.005

Publication date:
2005

Available online at www.sciencedirect.com
SCIENCE DIRECT®
European Journal of Mechanics A/Solids 24 (2005) 740–756

Successively refined models for crack tip plasticity in polymer blends

K.G.W. Pijnenburg [a], Th. Seelig [b,*], E. van der Giessen [c]

[a] *Department of Mechanical Engineering, Delft University of Technology, 2628 CD Delft, The Netherlands*
[b] *Fraunhofer-Institute for Mechanics of Materials IWM, Woehlerstrasse 11, 79108 Freiburg, Germany*
[c] *Materials Science Center, University of Groningen, 9747 AG Groningen, The Netherlands*

Received 7 January 2005; accepted 26 April 2005

Available online 16 June 2005

Abstract

This paper is concerned with a comparative study of different, partly complementary micromechanical models for crack tip plasticity in polymer-rubber blends. It is experimentally well established that interspersion of micron-scale rubber particles into a polymer matrix can lead to a significantly enhanced toughness of the material. The last two decades have witnessed growing consensus about the underlying mechanisms: particle cavitation, void growth, crazing, and shear yielding. Cavitation of the particles followed by massive shear yielding of the matrix and the resulting dissipation of energy is believed to give blends their improved toughness. At the very microlevel, i.e. at length scales of the order of the micron-sized rubber particles, the key damage processes are well identified and largely understood. Their effect on the macroscopic scale may well be captured in a homogenized sense by continuum models, e.g. of the Gurson-type when focusing on void growth. However, at the scale of a crack, a complete and tractable model incorporating all relevant deformation mechanisms is not yet available. On the one hand, strong gradients of the stress fields violate the assumption of a sufficiently homogeneous material for a continuum representation to be valid, while on the other hand the length scale involved is too large in practice to model all particles individually. Therefore, in this paper several models for crack-tip plasticity in blends are combined and compared. Although none of the models introduced pretends to be the final answer, they all shed some light on parts of the solution.

Keywords: Polymer blends; Rubber cavitation; Shear banding; Plastic dilatancy; Crack tip fields; Toughening mechanisms

1. Introduction

Blending with finely dispersed rubber particles is a well-known method to improve the fracture toughness of amorphous polymers (‘rubber toughening’) and has over the past decades led to a number of new materials that are now widespread in practical applications. Prominent examples are HIPS (high-impact polystyrene) or ABS (acrylonitrile–butadiene–styrene), but rubber toughening has also been successfully applied to other glassy polymers such as PC (polycarbonate) and PMMA (polymethylmethacrylate), see e.g. Bucknall (1977). The common underlying principle is the cavitation of the rubber particles in

* Corresponding author. Tel.: +49 761 5142 276; fax: +49 761 5142 110.
E-mail address: see@iwm.fhg.de (Th. Seelig).

0997-7538/$ – see front matter
doi:10.1016/j.euromechsol.2005.04.005

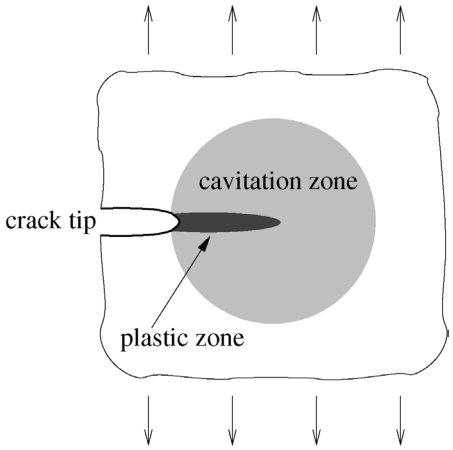

Fig. 1. Sketch of a typical stress-whitening zone in ABS, comprising a cavitation zone that encapsulates the plastic zone.

regions of high triaxial stress, and the subsequent initiation of inelastic matrix deformation leading to an enhanced energy dissipation.

The different inelastic deformation mechanisms enabled by cavitation of the rubber particles are void growth, shear yielding and distributed crazing. Their competition or cooperation depends on the material at hand, its microstructural features as well as on the loading conditions. In ABS, for instance, a size effect on toughening has been reported by Donald and Kramer (1982), which is due to small rubber particles leading to matrix shear yielding whereas larger ones promote crazing. Macroscopically, void growth, shear yielding and crazing become visible by a zone of so-called 'stress whitening' that develops near a crack tip before and during propagation. As illustrated in Fig. 1, two regions of this zone can be distinguished (Ni et al., 1991; Sue and Yee, 1996; Steenbrink et al., 1994). A circular zone of only diffuse stress whitening is ascribed to rubber cavitation alone, while in the zone of intense stress whitening massive matrix yielding and/or crazing takes place in addition. This plastic zone is well contained in the cavitation zone and exhibits a characteristic elongated shape ahead of the crack (Fig. 1).

With its elongated shape, the plastic zone typically observed in ABS is distinctly different from the shear band pattern characteristic for homogeneous glassy polymers (e.g. Ishikawa, 1995; Lai and van der Giessen, 1997). A possible reason for such an elongated shape is plastic dilatation due to distributed void growth and multiple crazing, but details are quite unclear at the moment. Also the origin of the particle-size effect in ABS is unclear. It is the aim of the present work to gain some better understanding of how the different micromechanisms mentioned above contribute to crack-tip plasticity in polymer-rubber blends. The experimental observation made for ABS by Steenbrink et al. (1994) that the thickness of the plastic zone correlates with the fracture toughness makes this understanding desirable from a practical point of view.

A number of theoretical studies have been performed to explore the role of rubber particle cavitation and matrix plasticity in the process of toughening. Approaches considering the situation at a crack tip typically take into account only the effect of a single particle or make use of a simplified description of the material behavior (e.g. Sue and Yee, 1996; Chen and Mai, 1999). Based on a more realistic constitutive model for glassy polymers and employing periodic cell models for blends under uniform macroscopic loading, another class of investigations focused on the yield processes in the matrix around cavitated rubber particles (e.g. Steenbrink and van der Giessen, 1999; Pijnenburg et al., 1999; Socrate and Boyce, 2000; Danielsson et al., 2002). These studies have shown that the deformation modes are strongly affected by the characteristic softening-rehardening behavior of glassy polymers, which leads to shear banding between the particles in blends. For the understanding of crack-tip plasticity in polymer-rubber blends, however, it seems necessary to combine both a realistic constitutive description *and* a large number of particles interacting with a crack tip in one model. In view of the fact that the typical notch radius (initial crack tip) in a fracture test specimen is several orders of magnitude larger than the (submicron) size of the rubber particles a straightforward finite element (FE) discretization would lead to as yet untractable numerical expenses. Approximations therefore have to be made, and different complementary approaches are followed in the present work.

First, Section 2.1 recapitulates some main results from the literature that will be used as starting points for the various models to be discussed. This includes a full constitutive model for glassy polymers as it has evolved over recent years. Also, the formulation of the particular two-dimensional crack-tip problem we look at is presented. Subsequent sections will then focus on several ways to tackle the problem of modeling the blend microstructure from different perspectives. One rather obvious model would be to homogenize the available micro models and apply them in the region close to the crack tip. This is what is done in Section 3 using a homogenized model where, for the moment, the possible effect of large stress or strain gradients on the homogenization assumption is ignored. Special attention will be given to plastic dilatancy due to void growth and its effect on

the mechanical response. It will be shown that dilatancy can have a serious influence on the predictions, thereby marking void growth as an important ingredient for a deeper understanding of crack-tip plasticity. In Section 4 we consider a coarse-grained model of the matrix-particle microstructure focusing on localized shear deformations in between particles. Plasticity is then handled by special surface elements representing the ligaments between neighboring particles. This enables large areas to be modeled, while still retaining most of the detail of the local nature of plasticity and microstructure. Cavitation, as a precursor to yielding, is included in this formulation, but void growth is excluded. Results show a high tendency for plastic deformation to localize in a rather diffuse zone, much smaller than the corresponding cavitation zone, incorporating a few dozens of particles. The last and by far most ambitious model is one where the crack tip and every single rubber particle in its neighborhood are represented explicitly (Section 5). In such a model both volumetric yielding and localized plasticity can be investigated at the same time, but for practical reasons it is limited to accounting for only a dozen of particles interacting with the crack.

Another limitation with regard to a realistic blend modeling, shared by all three approaches presented here, is the assumption of a well dispersed distribution of particles. In real blends agglomerations of particles are frequently observed which may have a strong effect on the overall performance.

2. Background models and problem formulation

2.1. Constitutive equations

Understanding plasticity of polymer-rubber blends requires knowledge of both the yield behavior of the thermoplastic matrix as well as the effect of microstructure. The different micromechanical blend models to be discussed in later sections adopt a common constitutive description of the matrix elastic-viscoplastic behavior of homogeneous glassy polymers. Originally proposed by Boyce et al. (1988) and modified by Wu and van der Giessen (1996), the model has been successfully applied to predict many aspects of the large strain deformation behavior of thermoplastics.

The model, which is only briefly summarized here, makes use of the standard additive decomposition of the rate of deformation tensor into its elastic and plastic parts: $\boldsymbol{D} = \boldsymbol{D}^{\mathrm{e}} + \boldsymbol{D}^{\mathrm{p}}$. The small strain elastic response is given by

$$\boldsymbol{D}^{\mathrm{e}} = \boldsymbol{\mathcal{L}}^{-1} \overset{\nabla}{\boldsymbol{\sigma}}, \tag{1}$$

where $\overset{\nabla}{\boldsymbol{\sigma}}$ is the Jaumann rate of the Cauchy stress and $\boldsymbol{\mathcal{L}}$ is the standard fourth-order isotropic elasticity tensor in terms of Young's modulus E and Poisson's ratio ν. The isochoric viscoplastic strain rate

$$\boldsymbol{D}^{\mathrm{p}} = \frac{\dot{\gamma}^{\mathrm{p}}}{\sqrt{2}} \frac{\bar{\boldsymbol{\sigma}}'}{\tau} \tag{2}$$

is specified in terms of the equivalent plastic shear strain rate $\dot{\gamma}^{\mathrm{p}} = \sqrt{\boldsymbol{D}^{\mathrm{p}} \cdot \boldsymbol{D}^{\mathrm{p}}}$ and the deviatoric driving stress $\bar{\boldsymbol{\sigma}}'$ normalized by the equivalent driving shear stress $\tau = \sqrt{\frac{1}{2}\bar{\boldsymbol{\sigma}}' \cdot \bar{\boldsymbol{\sigma}}'}$. The latter serves to determine $\dot{\gamma}^{\mathrm{p}}$ via Argon's law (see Boyce et al., 1988) expression

$$\dot{\gamma}^{\mathrm{p}} = \dot{\gamma}_0 \exp\left[-\frac{A\tilde{s}}{T}\left(1 - \left(\frac{\tau}{\tilde{s}}\right)^{5/6}\right)\right] \tag{3}$$

where $\dot{\gamma}_0$ and A are material parameters, and T is the absolute temperature (constant in the present analyzes). In order to phenomenologically model the intrinsic softening of the glassy polymer, the shear resistance $\tilde{s}$ in (3) is taken to evolve with plastic strain according to

$$\tilde{s}(\gamma^{\mathrm{p}}) = s_s + (s_0 - s_s)\exp(-h\gamma^{\mathrm{p}}/s_s) - \alpha\sigma_m \tag{4}$$

from an initial value s_0 to a saturation value s_s (Boyce et al., 1988). Furthermore, it incorporates (via the constant pre-factor α) a dependence on the hydrostatic stress $\sigma_m = \frac{1}{3}\operatorname{tr}\boldsymbol{\sigma}$ to capture the pressure sensitivity of the yield strength of glassy polymers. Post-yield progressive hardening at large stretches is due to alignment of the molecular network and is described by the back stress tensor $\boldsymbol{b}$ incorporated in the driving stress $\bar{\boldsymbol{\sigma}}' = \boldsymbol{\sigma}' - \boldsymbol{b}$. Drawing on the analogy with cross-linked rubber (Arruda and Boyce, 1993) the principal components of the back stress tensor are specified in terms of principal stretches. This back stress model involves two material parameters: the initial hardening modulus C_R and the limit stretch of the molecular chains $\lambda_{\max}$ at which the network 'locks' and no further yielding is possible. The set of material parameters listed in Table 1 is representative of SAN (styrene–acrylonitrile), the thermoplastic matrix in ABS. Full details of the constitutive model may be found in (Wu and van der Giessen, 1996).

The constitutive behavior of the rubber particles will not be explicitly accounted for in the various blend models to be introduced in subsequent sections. The main impact of the rubber particles on the behavior of the blend is understood to be

Table 1
Material parameters used for SAN in the present study

	E/s_0	ν	$\dot{\gamma}_0$ [sec^{-1}]	s_s/s_0	As_0/T	h/s_0	α	$\lambda_{\max}$	C_R/s_0
SAN	12.5	0.38	1.06×10^8	0.79	52.2	12.6	0.25	3.5	0.033

due to their cavitation, after which they can be regarded mechanically equivalent to voids. Previous theoretical studies (see e.g. Steenbrink and van der Giessen, 1997, 1999) have shown that cavitation of a rubber particle under purely hydrostatic stress takes place when the hydrostatic stress inside the particle reaches 2.5 times the shear modulus of the rubber. Since rubber particle cavitation in real blends also depends on the matrix material, the stress triaxiality and pre-existing flaws, the assumption is made here that cavitation takes place at a critical mean stress σ_m^{cav}, the value of which is to be determined from experiments (see, e.g., Ramaswamy and Lesser, 2002).

2.2. Problem formulation

Inelastic deformation at crack tips in polymer blends is typically confined in a small zone, here referred to as the 'process zone' because of the various mechanisms involved. Therefore a small-scale yielding (or damage) assumption can be made, which allows to model only the region dominated by the elastic K-field inside which the much smaller process zone is contained. Mode I crack-tip loading is specified in terms of the corresponding displacements or tractions for a sharp crack as far-field boundary conditions (Fig. 2). Further details on this type of problem setting may be found e.g. in Lai and van der Giessen (1997) where crack-tip plasticity in homogeneous glassy polymers has been investigated.

The focus here is on the development of crack-tip plasticity in polymer-rubber blends prior to crack growth when, according to experiments for ABS (Steenbrink et al., 1994), the major part of the total fracture energy is dissipated. Therefore, a stationary blunted crack tip is considered and loading is specified in terms of the applied far-field mode I stress intensity factor K_I which is normalized as $\overline{K} = K_I/s_0\sqrt{r_{\text{tip}}}$ throughout the paper. Here, $s_0 = 120$ MPa is the initial yield strength of SAN, and r_{tip} denotes the initial crack tip radius. A constant loading rate of $\dot{\overline{K}} \approx 10$ sec^{-1} is applied; the effect of loading rate is not investigated here. The volume fraction of rubber particles is taken to be $f_0 = 0.25$ which is a typical value for commercial ABS. Inside the process zone (Fig. 2) cavitation of the rubber particles and massive yielding of the surrounding matrix are expected to take place. Rubber cavitation is assumed to take place at a realistic value of $\sigma_m^{\text{cav}} = 18$ MPa. The occurrence of particle cavitation and the subsequent evolution of the cavitation zone in the course of loading will be an outcome of the full analysis.

The numerical treatment follows the method described by Wu and van der Giessen (1996) and employs a Total Lagrangian formulation of the finite deformation boundary value problem and a rate-tangent integration of the constitutive equations (Pierce et al., 1984). Modifications of the method arising from the different blend models will be discussed in the respective sections. The analyzes are carried out for plane strain conditions and symmetry of the (mode I) problem is exploited.

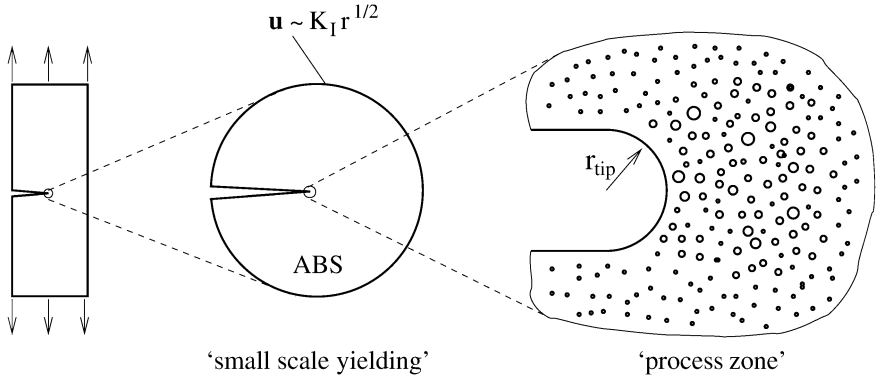

Fig. 2. Crack-tip modeling in ABS.

3. Fully homogenized model

3.1. Continuum modeling of porous glassy polymers

One way to simplify the description of the blend material is to smear out its two-phase microstructure and represent it by a homogenized effective medium. The response of this continuous ABS model is taken to consist of two regimes separated by the event of rubber cavitation which takes place at a critical mean stress σ_m^{cav}. Prior to cavitation, the elastic rubber particles of volume fraction f_0 sustain hydrostatic stress and the effective medium behaves plastically incompressible. After cavitation, the rubber particles are considered mechanically equivalent to voids and the overall behavior of ABS is approximated by that of porous SAN. The porosity f then enters the second regime of the model as an additional variable with its initial value f_0 reflecting the rubber content in the blend. Due to the plastically incompressible matrix behavior (Section 2.1), for small elastic strains the evolution of porosity after rubber cavitation is governed by the volumetric part of the plastic strain rate in the porous material according to

$$\dot{f} = (1-f)\,\mathrm{tr}\,\boldsymbol{D}^{\mathrm{p}}. \tag{5}$$

The overall elastic behavior of ABS before and after rubber cavitation is assumed to be isotropic and is described by effective elastic constants E^* and ν^*. Since the shear modulus of rubber is small compared to that of SAN it can be neglected at all. The bulk modulus of rubber is approximately of the same order as that of SAN; for simplicity it is taken equal to it before cavitation, while afterwards it is set to zero. Expressions for E^* and ν^* in terms of E and ν of the SAN matrix and the porosity f can be found in Pijnenburg and van der Giessen (2003).

Based on the yield behavior of the SAN matrix described by the constitutive model in Section 2.1, the effective ABS response is taken to be plastically incompressible before cavitation. After cavitation it exhibits plastic dilatancy under hydrostatic stress corresponding to an increasing porosity (i.e. void growth in a real blend). Numerous porous plasticity models have been suggested in the literature, starting from the original model by Gurson (1977) for volumetric yielding in a porous material with a rigid perfectly plastic matrix, which has later been extended by others for more general material behavior. With a special view on the characteristic features of glassy polymers, Steenbrink et al. (1998) and Pijnenburg and van der Giessen (2001) developed a model that exhibits much better agreement with voided cell calculations than the unmodified Gurson model. However, for computational convenience, the following purely phenomenological yield function is adopted here:

$$\Phi \equiv \frac{1}{2}\bar{\boldsymbol{\sigma}}' \cdot \bar{\boldsymbol{\sigma}}' + a f_0{}^b \sigma_m^2 - \left[(1-f)\tau c(f_0)\right]^2. \tag{6}$$

This condition differs from the Gurson (1977) and the Pijnenburg–Van der Giessen (2001) models in the dependence on hydrostatic stress and (initial) void volume fraction. The influence of hydrostatic stress in conjunction with the initial porosity f_0 is considered to be 'collapsed' into the 'free' parameters a and b. From comparison with the response of a representative volume element of SAN containing a number of explicitly modeled voids, these parameters have been fitted to values of $a = 1$ and $b = 0.7$ by Seelig and van der Giessen (2002). Prior to cavitation, volumetric yielding is precluded by setting $a = 0$. When the hydrostatic stress reaches the critical value σ_m^{cav} in the course of loading, 'cavitation' takes place and the transition from uncavitated to cavitated effective elastic constants and from $a = 0$ to $a = 1$ in the yield potential (6) is carried out over a small number of time steps. Due to the intrinsic softening of SAN, plastic flow at the onset of macroscopic yield is not uniformly distributed throughout the matrix phase but localizes in ligaments connecting neighboring voids (Pijnenburg et al., 1999). Therefore, at $f = f_0$ the driving stress τ should scale with the relative width of the intervoid ligament instead of with the matrix volume fraction. This effect and its dependence on the initial porosity is accounted for by the term $c(f_0)$, which from simple analytical considerations can be approximated by $c(f_0) = (1+\sqrt{f_0})^{-1}$ for the 2D case of cylindrical voids (Pijnenburg and van der Giessen, 2001; Seelig and van der Giessen, 2002).

The plastic strain rate is obtained from the (normality) flow rule

$$\boldsymbol{D}^{\mathrm{p}} = \lambda \frac{\partial \Phi}{\partial \bar{\boldsymbol{\sigma}}}, \tag{7}$$

where the multiplier λ is determined by the condition that the dissipation per unit deformed volume of the porous material equals the dissipation in the matrix:

$$\bar{\boldsymbol{\sigma}} \cdot \boldsymbol{D}^{\mathrm{p}} = (1-f)\sqrt{2}\tau\dot{\gamma}^{\mathrm{p}}. \tag{8}$$

The equivalent driving stress τ, determined from $\Phi = 0$, together with the equivalent plastic strain rate $\dot{\gamma}^{\mathrm{p}}$ obtained from inserting τ into (3) represents the 'effective' viscoplastic behavior of the whole matrix phase (Steenbrink et al., 1998). Correspondingly, (4) describes the effective shear resistance of the matrix in the homogenized porous medium and is, by virtue of its pressure sensitivity, taken to depend on the average hydrostatic matrix stress $\sigma_m^{\text{matrix}} = \sigma_m/(1-f)$. Because of the highly nonuniform distribution of plastic flow in the matrix phase of a voided glassy polymer, intrinsic

softening of the material is evened out in the overall response (Smit et al., 1999; Pijnenburg and van der Giessen, 2001; Seelig and van der Giessen, 2002). To incorporate this effect in the homogenized model, the amount of intrinsic softening, i.e. the difference $s_0 - s_s$ in (4), is taken to decrease linearly with increasing rubber content f_0 and to vanish for $f_0 \geqslant 0.3$. From the few experimental data in the literature (e.g. Ishikawa, 1995) as well as from the above-mentioned simulations it remains rather unclear how the overall hardening behavior of ABS is affected by the matrix hardening in conjunction with the heterogeneous microstructure. As a first approximation, therefore, we take the values of the hardening modulus C_R and the limit stretch $\lambda_{\max}$ of SAN to apply also to ABS in the present model.

3.2. Results

The evolution of the plastic zone near a crack tip in ABS according to the model described above is presented in Fig. 3 in terms of the equivalent plastic strain rate $\dot{\gamma}^{\mathrm{p}}$ at levels of the normalized stress intensity factor of $\bar{K} = 0.8$ and 1.2. Also shown is the zone inside which cavitation has taken place and which is already large compared to the plastic zone in the early stage of loading (Fig. 3(a)). Nevertheless, even at higher load levels the cavitation zone remains well contained in the total region analyzed (center of Fig. 2) such that the small-scale yielding assumption still holds. From Fig. 3(b) it can clearly be seen how the plastic zone spreading ahead of the crack tip develops into an elongated shape and localizes in front of the crack. The simulation reveals that yielding there is essentially volumetric. Hence, the localization in a 'dilatational band' results from the volumetric softening exhibited by the homogenized ABS model (Seelig and van der Giessen, 2002). Although the elongated shape of the plastic zone obtained from the simulation is qualitatively similar to that observed in experiments (e.g. Steenbrink et al., 1994) it has to be noted that the porosity in its core region in Fig. 3(b) attains an unrealistically high value of $f \approx 70\%$. Furthermore, volumetric softening and localization lead to a plastic zone width which seems too narrow compared to real ABS and in addition introduce a mesh dependence into the numerical model.

The distribution of hydrostatic stress shown in Fig. 4 is normalized by the initial yield stress s_0 of neat SAN and correlates with the shape of the plastic zone. The peak value of hydrostatic stress is located straight ahead of the zone of intense volumetric yielding and is 'pushed' further away from the crack tip by the propagation of the plastic zone in the course of loading. Due to the increasing porosity and volumetric softening inside the elongated plastic zone, a region of low hydrostatic stress (bright grey) develops between the notch root and the location of peak hydrostatic stress (Fig. 4(b)). Right at the location of peak hydrostatic stress, however, the porosity has not yet changed much from its initial value, so that the volumetric softening has not occurred and a relatively high hydrostatic stress can still be maintained. This location coincides with the small egg-shaped region at the tip of the elongated plastic zone in Fig. 3(b) where yielding takes place in a spatially more distributed manner than in the main localized part of the plastic zone closer to the notch. This indicates an increasing tendency for localization of plastic flow with increasing porosity.

Comparison of the above results in terms of porosities obtained from the simulations with micrographic analyzes of real ABS (e.g. Steenbrink et al., 1994; Jar et al., 2002) indicates that the assumption of the total rubber content being converted into porosity leads to an overestimation of plastic dilatancy with an unrealistically high tendency for localization of volumetric

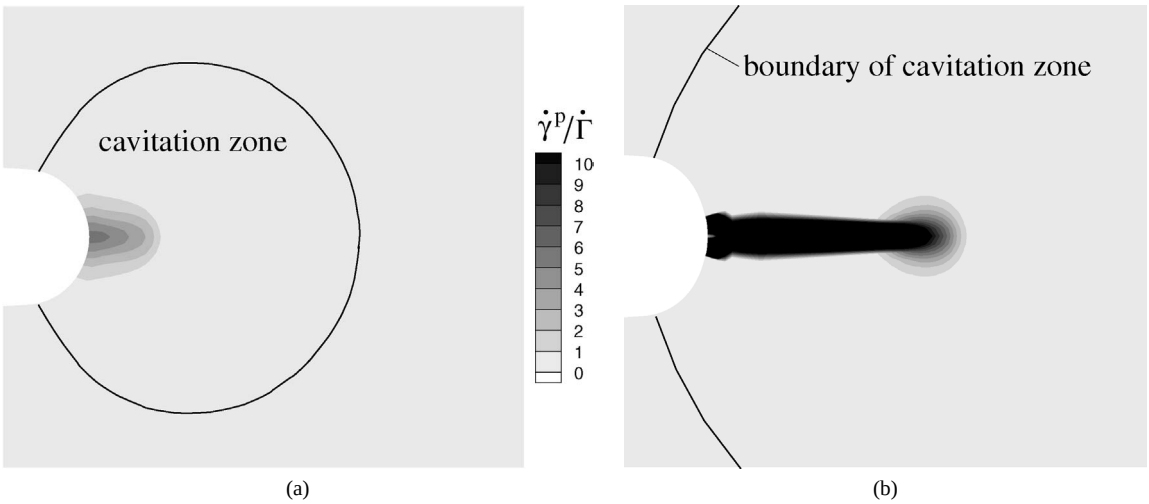

Fig. 3. Equivalent plastic strain rate $\dot{\gamma}^{\mathrm{p}}$ (normalized by $\dot{\Gamma} = 0.1\dot{K}_I/s_0\sqrt{r_{\mathrm{tip}}}$) and cavitation zone according to homogenized porous plasticity model at load levels (a) $\overline{K} = 0.8$ and (b) $\overline{K} = 1.2$.

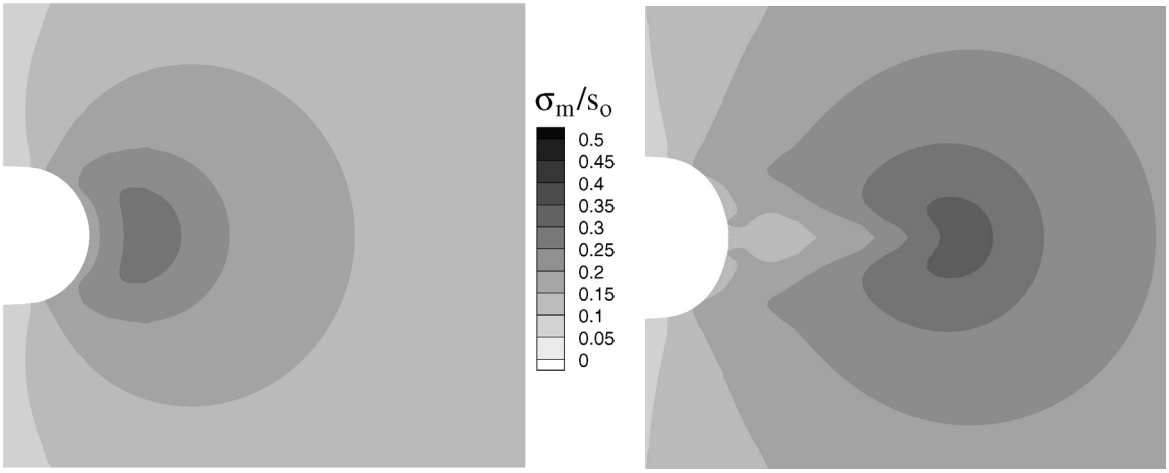

Fig. 4. Distribution of hydrostatic stress according to homogenized porous plasticity model at (a) $\overline{K} = 0.8$ and (b) $\overline{K} = 1.2$.

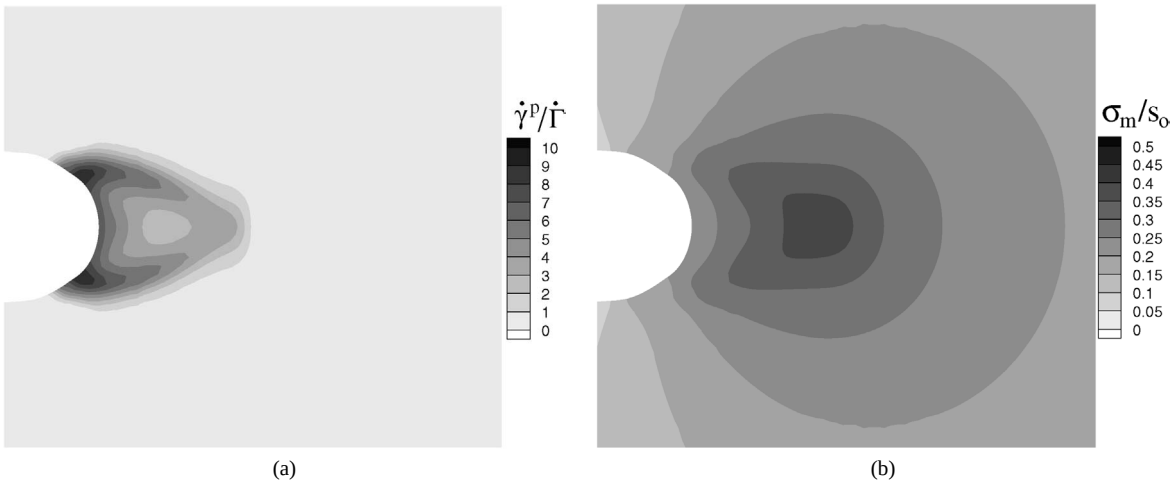

Fig. 5. Equivalent plastic strain rate (a) and hydrostatic stress (b) at $\overline{K} = 1.2$ according to homogenized model without plastic dilatancy and enhanced mean stress sensitivity $\alpha = 0.75$.

yield. In contrast to this localization of void growth predicted by the present model, void growth from cavitated rubber particles in real ABS occurs rather uniformly dispersed over regions that are large compared to the particle size even close to a fracture surface (Jar et al., 2002). As another extreme case of a homogenized ABS model therefore we now neglect volumetric yield at all and instead account for the presence of cavitated rubber particles only through an enhanced dependence of the yield stress on the hydrostatic stress. This is accomplished by setting $a = 0$ in (6), so that $\mathrm{tr}\,\boldsymbol{D}^{\mathrm{p}} = 0$ from (7), while a value $\alpha = 0.75$ in (4) is chosen (Table 1). The three-times higher value of α is chosen for reasons to be explained in Section 4.1. Evidently, the assumption of plastic incompressibility of the blend material is not very realistic; it here serves merely to separate the effect of plastic dilatancy from pure shear yielding. Fig. 5 shows the distribution of equivalent plastic strain rate and hydrostatic stress at a load level of $\overline{K} = 1.2$, to be compared with Figs. 3(b) and 4(b), respectively. The plastic zone in Fig. 5(a) differs significantly from that of the plastically dilatant material model (Fig. 3(b)). Maximum values of plastic strain rate now are obtained in shear bands initiated at the notch and intersecting at some distance ahead of it. As expected, hydrostatic stresses are higher in the plastically incompressible material (Fig. 5(b)). The distribution of plastic strain rate and hydrostatic stress, with a peak of the latter at the location of intersecting shear bands, resembles that in neat thermoplastics found by Lai and van der Giessen (1997). Compared to their results, contours in the present case are more elongated due to the enhanced influence of mean stress on plastic flow. This effect has also been observed by Jeong et al. (1994) in a slip line analysis of a pressure dependent perfectly plastic material.

The evolution of the cavitation zone as indicated in Fig. 3 is not affected by the above modification of the model since its size is much larger than the plastic zone. This means that the processes of rubber cavitation and plastic matrix flow are effectively decoupled in the present model. However, at crack tips in real ABS, a stronger interaction between cavitation and plastic flow cannot be ruled out because certain blend manufacturing processes may result in a higher rubber cavitation resistance than the value of σ_m^{cav} assumed here (Jar et al., 2002). As another shortcoming, it should be noted that a homogenized model for the blend material is strictly valid only in situations where a sufficiently large number of heterogeneities is subjected to macroscopically uniform loading. At a crack tip this is clearly not the case, and it therefore may be important to account explicitly for the interaction of individual particles or voids among each other and with the crack tip.

4. Shear surface modeling

Detailed calculations of voids do capture their interactions with the crack tip, but are too costly in terms of computing power to extend to more than a handful of particles (cf. Section 5). The shear surface model introduced by Pijnenburg and van der Giessen (2003) was born from the wish to find a compromise between the two conflicting interests (i.e. size and detail) and close the gap between the models. The motivation for the shear surfaces originates from detailed finite element studies of regular arrays of voids, examples of which are shown in Fig. 6. From these calculations it was observed that most of the material deforms elastically, while the specific plastic material behavior is expressed only in small actively deforming zones, shear bands, that connect neighboring voids. Moreover, the location of these zones appears to be determined as much by the relative position of the voids as by the loading itself. In other words, knowledge of the microstructure of the material tells us where plastic deformation *might* take place, while (local) loading conditions determine where plasticity actually *will* take place.

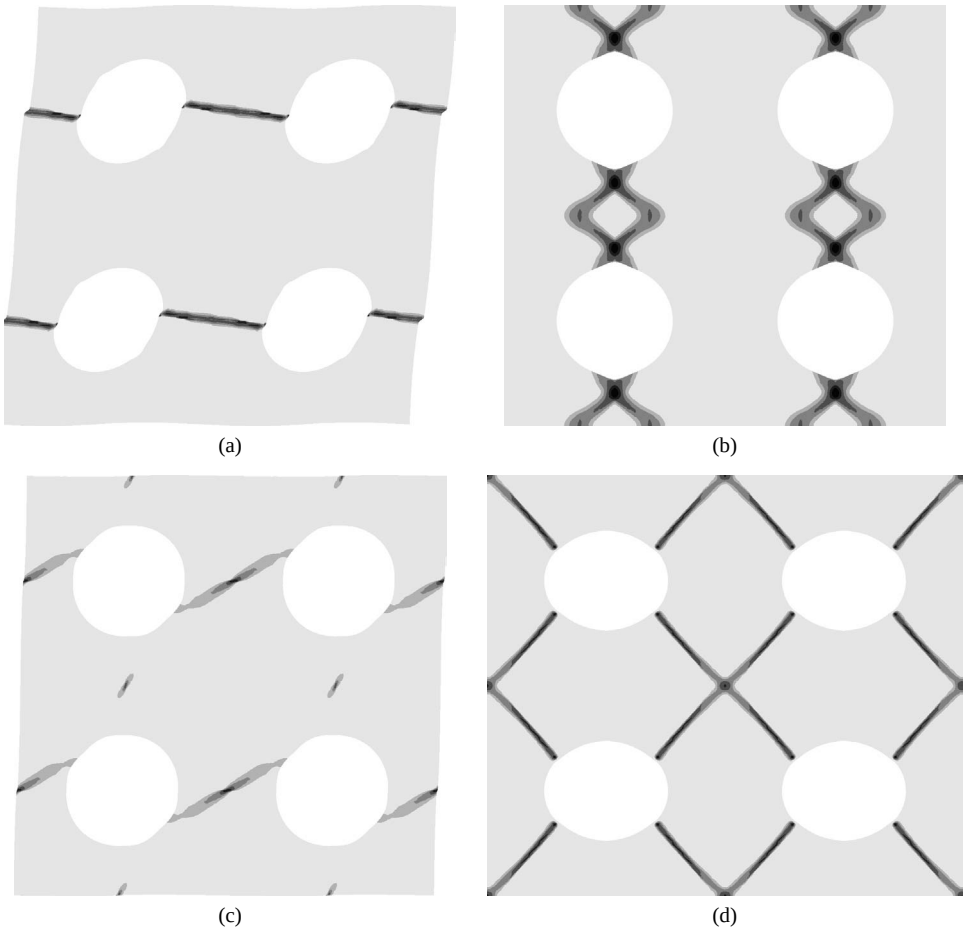

Fig. 6. Finite element simulations of a square array of voids under different loading conditions. The grayscales highlight the areas were plastic activity takes place, as measured by $\dot{\gamma}^{\text{p}}$. (a) simple shear, (b) uniaxial tension, (c) simple shear combined with biaxial tension and (d) pure shear.

The notion that with each microstructure is connected a limited number of possible deformation zones, provides us with a way to devote computational efforts to those regions where it is most needed.

To illustrate the above ideas look again at the detailed FE simulations in Fig. 6. They show the distribution of plastic strain rate in an advanced stage of deformation. Clearly it can be seen that in all cases most plastic activity is taking place in well defined shear bands connecting neighboring particles. Exactly which band (horizontal, vertical or diagonal) will be activated is determined by the loading conditions. In the relatively simple situations (i.e. a periodic square array of voids and uniform loading) shown in Fig. 6 one would be able to predict which mode of deformation will be activated. In more general and therefore more complicated microstructural or loading situations this will not always be possible. Nevertheless, we do expect localized shearing to take place in the ligaments between neighboring voids. So, our focus should be upon these ligaments; the shear surface model does exactly this. Special surface elements representing the ligaments are situated along the lines connecting particles, while the remaining space is filled with regular elastic triangular elements (see Fig. 7). The surface elements serve to capture all plastic deformation in a condensed and simplified way. Any plasticity that takes place in the zone between two voids is collapsed into two sliding surfaces, where the shear traction τ is related to the relative shear displacement Δ_t. The relation between the two is chosen in such a way that it mimics the average (large scale) material behavior of the full-scale, detailed FE simulations. The details of the method have been described in Pijnenburg and van der Giessen (2003). Suffice it here to recapitulate the main results.

Fig. 7(b) depicts a shear surface in detail. It is mainly characterized by its direction $\boldsymbol{t}$, the unit normal $\boldsymbol{n}$ and the length l of the ligament between two adjacent voids with equal radius r_v. Initially, the node pairs $(1, 3)$ and $(2, 4)$ will coincide with the two respective void centers. The degrees of freedom of a shear surface are the relative displacements $\boldsymbol{\Delta}_i$ $(i = 1, 2)$ of the node pairs. The components in $\boldsymbol{n}$ and $\boldsymbol{t}$-direction give the normal opening and tangential sliding of the two faces with respect to each other.

The conjugate tractions τ and σ have to follow from integration of a suitable constitutive equation along the ligament. For our purpose, only shear deformations will be important. The normal opening should therefore be kept as low as possible. The easiest way to ensure that is by giving the shear surface a high stiffness against normal displacements (see Pijnenburg and van der Giessen, 2003), i.e.

$$\sigma = \frac{c}{r_v} E \Delta_n, \tag{9}$$

where E is the Young's modulus of the matrix and c is an adjustable multiplication factor. The value used here is $c = 100$, which proved high enough to keep the normal opening sufficiently small, while at the same time being low enough not to cause numerical problems. The void radius r_v is introduced for dimensional reasons only. The constitutive relation for τ was constructed in such a way that it approximates the response of a shear band between voids as predicted by detailed finite element studies. The material description in the latter kind of studies (see discussion in Section 2.1) features elastic-viscoplasticity, with softening immediately after yield and re-hardening at large strains. These features served as heuristic basis for the constitutive equation for a shear surface. In analogy with the continuum formulation, the shear displacement Δ_t is split into an elastic, Δ_t^{e}, and a plastic part, Δ_t^{p}. For the elastic part, we write

$$\dot{\tau} = \frac{\zeta}{r_v} G \dot{\Delta}_t^{\mathrm{e}} = \frac{\zeta}{r_v} G \big(\dot{\Delta}_t - \dot{\Delta}_t^{\mathrm{p}}\big) \tag{10}$$

where $G = E/2(1 + \nu)$ is the shear modulus of the bulk. The dimensionless coefficient ζ serves as a fitting factor to keep the elastic shear displacements low. This is necessary to prevent the introduction of shear surfaces in between bulk elements from increasing the overall compliance of the blend (the analogous effect in embedded cohesive zones is well known, see e.g. Xu and Needleman, 1994; Tijssens et al., 2000). Although a large ζ value would result in small additional compliance, the corresponding stiffness of the shear surfaces would deteriorate the condition of the final overall stiffness matrix. A compromise was found (Pijnenburg and van der Giessen, 2003) by using $\zeta = 50$. The plastic part of the shear velocity $\dot{\Delta}_t^{\mathrm{p}}$ is expressed in the form

$$\dot{\Delta}_t^{\mathrm{p}} = \beta r_v \dot{\gamma}^{\mathrm{p}}, \tag{11}$$

where $\dot{\gamma}^{\mathrm{p}}$ is a plastic shear strain rate. Here again the void radius r_v ensures dimensional consistency. The coefficient β serves to adjust the stress value at which plastic flow starts. Writing (11) in this form enables us to employ the same constitutive framework (3), (4) as used in the continuum viscoplasticity model. The value of the material parameters is of course different from that in the continuum formulation, since some details of the local variations around the voids is lost in the shear surface model. We also take a somewhat different (simpler) description of the back stress $\boldsymbol{b}$, describing the hardening taking place inside the shear band due to the stretching of the molecules. Rather than the nonlinear hardening in the continuum model, the hardening relation τ_{h} used in the shear surface model is instead taken as a simple linear function of the shear displacement in the shear surface, i.e.

$$\tau_{\mathrm{h}} = C_{\mathrm{s}}^{\mathrm{R}} \Delta_t, \tag{12}$$

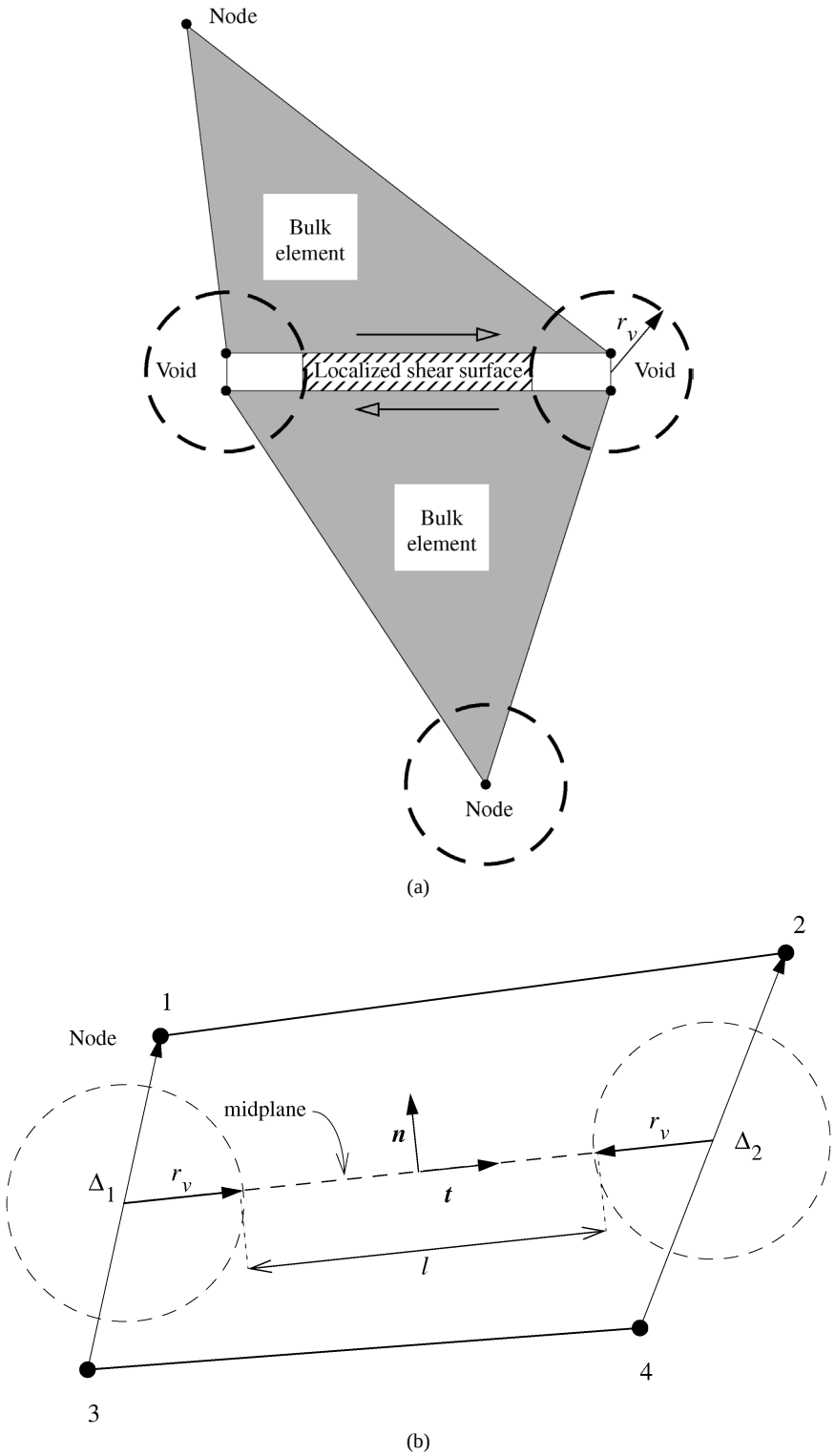

Fig. 7. (a) Schematic overview of two triangular bulk elements and corresponding 'shear surface' in between two voids. (b) Enlarged view of a shear surface, showing all relevant parameters.

Table 2
Material parameters used in the shear surface model (SAN)

	E/s_0	ν	$\dot{\gamma}_0$ [sec^{-1}]	s_{ss}/s_0	As_0/T	h_s/s_0	α_s	C_s^R/s_0	ζ	β
SAN	12.6	0.38	1.06×10^8	0.79	52.2	126	0.75	1.05	50	50

with C_s^R the hardening modulus. This is justified by the observation (e.g. Steenbrink et al., 1998) that the process of shear band propagation in the ligament in between the voids smears out the local, nonlinear hardening to a more gradual one.

The constitutive response of a shear surface is reminiscent to that of the underlying bulk amorphous polymer under shear. Note however that in the shear surface model not all 'material' parameters have the same sound physical basis as before, nor have their values any relation to the original formulation. Besides the hardening modulus C_s^R and ζ and β, which control the overall elastic modulus and the yield point, also h_s, governing softening and α_s, related to pressure sensitivity, have been used as tunable parameters, which were fitted to detailed cell analyzes. The parameters used in the present study, summarized in Table 2, are the same as those determined in Pijnenburg and van der Giessen (2003), with one notable exception. Instead of using the value for α_s as determined in that study by fitting to cell calculations for low triaxialities, we here use a value found from fitting to an analytical yield curve, as will be explained below.

4.1. Pressure sensitivity

One limitation of the shear surface concept is that a single shear surface is only capable of describing plastic deformations that have a significant shearing component. Obviously, by construction, it will only allow for deformations parallel to its surface. Provided the region being analyzed is large enough to contain surface elements in all possible directions and loading is sufficiently uniform throughout, this will not pose a significant problem. Although also in such situations on very local scales (i.e. single surfaces) deformations are only possible along the surfaces, on a somewhat larger scale the combined deformation of several surfaces may provide the necessary freedom to accommodate induced plasticity in any direction. The behavior under hydrostatic stress is especially important since yield of glassy polymers shows strong pressure dependence, see the discussion after (4). Originally (Pijnenburg and van der Giessen, 2003) the pressure sensitivity parameter α_s was determined by fitting to detailed calculations for low triaxialities only. By contrast, we here use a random arrangement of 500 voids, as depicted in Fig. 8. The corresponding mesh, with shear surfaces in virtually all directions, is capable of deforming under general loading conditions and is used here to estimate the pressure sensitivity parameter, α_s. Due to the many voids represented and the random structure, direct comparison with detailed calculations has now become computationally expensive.

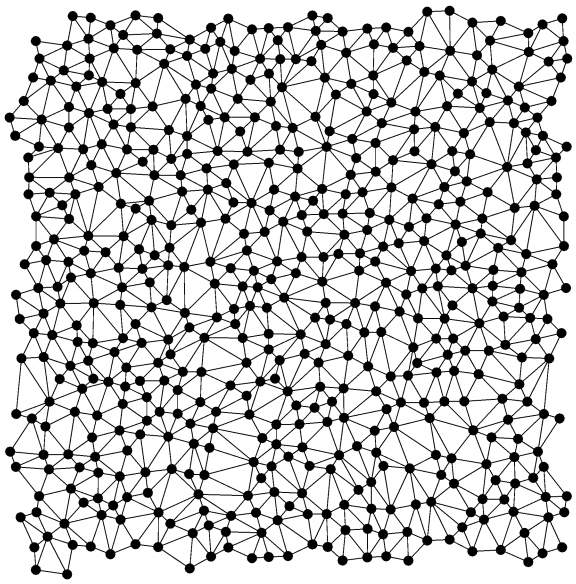

Fig. 8. Mesh used in pressure sensitivity analysis, consisting of 500 randomly distributed voids (black dots, only shown for clarity as they are not explicitly modeled) in a glassy polymer. The lines connecting neighboring particles define 'shear surfaces', cf. Fig. 7, while the triangles signify triangular bulk elements.

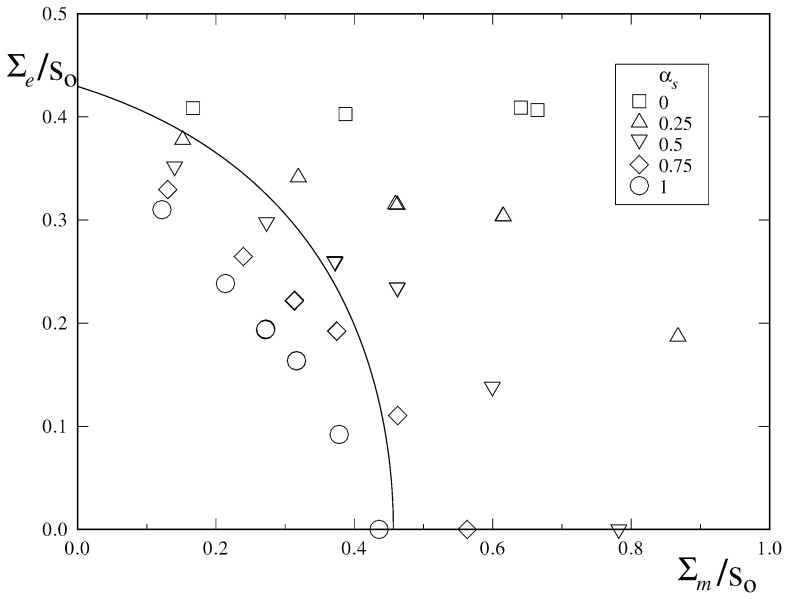

Fig. 9. Yield curves according to (solid line) the analytical model of Pijnenburg and van der Giessen (2001) and shear surface model for several values of α_s.

Fortunately, this can be circumvented by not comparing to detailed FE calculations, but to the approximate theoretical yield surface for a homogenized blend taken from Pijnenburg and van der Giessen (2001) (see also the discussion in Section 3.1). Fig. 9 shows the result of the analysis. In addition to the analytical yield locus (solid line), some yield points (as determined by the maximum in the stress–strain curve for the sample in Fig. 8) under different applied triaxialities are shown for various values of α_s. Although the shear surface model does not reproduce the analytical curve perfectly, a value of $\alpha_s = 0.75$ (as also used in Section 3.2) comes sufficiently close for the triaxiality range of interest in this study. This gives us confidence that also under high hydrostatic tension the model will capture most of the pressure sensitivity in an acceptable manner. Although other ways of implementing pressure sensitivity (for instance making α_s itself pressure dependent) are certainly conceivable, it is questionable whether this would significantly improve the results of the crack-tip problem. Preliminary investigations in this direction indicated no strong influence of the precise manner in which pressure sensitivity is accounted for.

4.2. Results

The shear surface model is now applied to the region around a crack tip. The radius r_v of the (equal-sized) voids is taken 20 times smaller than the crack tip radius; their average spacing is then determined by the void volume fraction $f_0 = 0.25$. As explained in Section 2.2 all plastic activity is expected to take place in the process zone, so that shear surfaces are used only there. During the first stage of loading the material in the process zone responds in an entirely elastic manner, since the shear surfaces are not allowed to undergo any (plastic) shear deformation as long as the rubber particles have not cavitated. As before, cavitation takes place at a (local) hydrostatic stress of $\sigma_m^{\text{cav}} = 18$ MPa. Once the particles at both ends of a shear surface have cavitated, the corresponding shear band is activated. If and how much plasticity will subsequently take place is then determined by the constitutive equations of the shear surfaces. By construction, all dissipative processes in the shear surface model take place in those surfaces. Since these are idealized elements of zero width, the elements and any plasticity therein would not be visible in a graphical representation unless special care is taken. Therefore, in the subsequent plots, the surfaces have been given a small finite width, so that the information contained in them can be rendered.

As in the continuum computations, Section 3, the cavitation zone grows much faster than the plastic zone. Plasticity seems to localize in the small region just in front of the crack tip. This is illustrated in Fig. 10(a), which shows both the cavitated zone in ABS with 25% rubber content at $\overline{K} = 0.8$ and the plastic strain rate $\dot{\gamma}^p$ in the shear surfaces (normalized as explained in caption of Fig. 3). Evidently, while the cavitation zone is already much larger than the crack tip radius, the plastic zone is still quite small. Plasticity localizes in two major bands that come together ahead of the crack tip. Perpendicular to this main structure two, less active, minor bands can be seen to develop. Fig. 10(b) shows the distribution of normalized hydrostatic stress in the region corresponding to that of Fig. 10(a). One can see that the hydrostatic stress peaks where the shear bands cross.

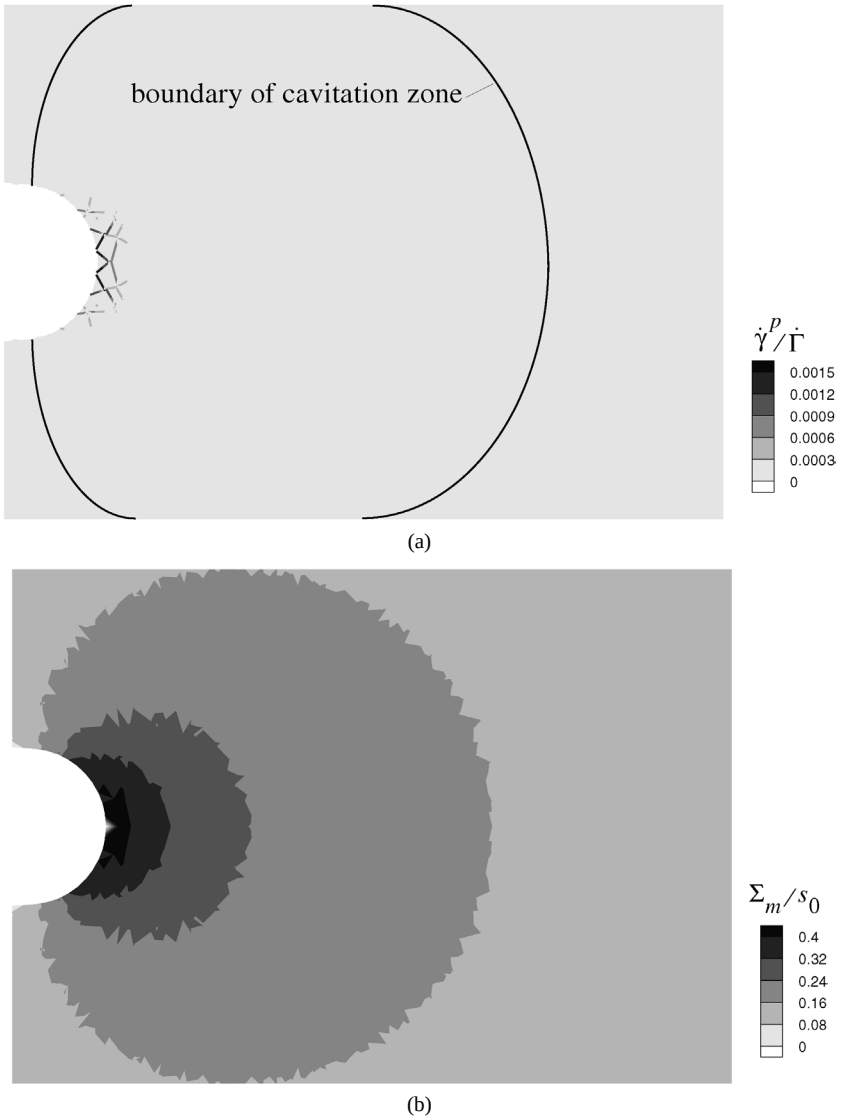

Fig. 10. (a) Plastic strain activity $\dot{\gamma}^p$ and cavitation zone at $\overline{K} = 0.8$ according to the shear-surface model; (b) Distribution of hydrostatic stress.

When the load is increased further, up to $\overline{K} = 1.2$, we obtain the situation as depicted in Fig. 11. Here, both the cavitation zone and the plastic zone have grown in size. The most active shear zone has propagated away from the crack tip and into the material. The hydrostatic stress, shown in Fig. 11(b), displays a similar behavior. The absolute values of peak stress did not grow as much, but zones with the same stress levels have grown significantly. Furthermore, the peak has shifted away from the crack tip. The results show some resemblance to the results in Fig. 5 obtained by the continuum model without plastic dilatation. At high loads, plasticity tends to localize in just a few shear surfaces where total strain reaches very high values. Surrounding bulk elements then do not have enough freedom to move so as to readily accommodate all of this deformation. Additional calculations where some key parameters (loading rate, crack tip size and rubber content) were varied show similar results. Shape and size of both the plastic zone and the cavitation zone are basically the same for these calculations. This could mean that the introduction of shear surfaces swamps all dependence on other factors. Alternatively, it might be that most of the distinctions will only show up at load levels that are not easily attainable with the present model.

5. Discrete void modeling

The fully homogenized model with plastic dilatancy (Section 3) and the discrete shear surface model (Section 4) can be regarded as extreme cases of models for real ABS since each of them focuses only on a single mechanism (volumetric yield or

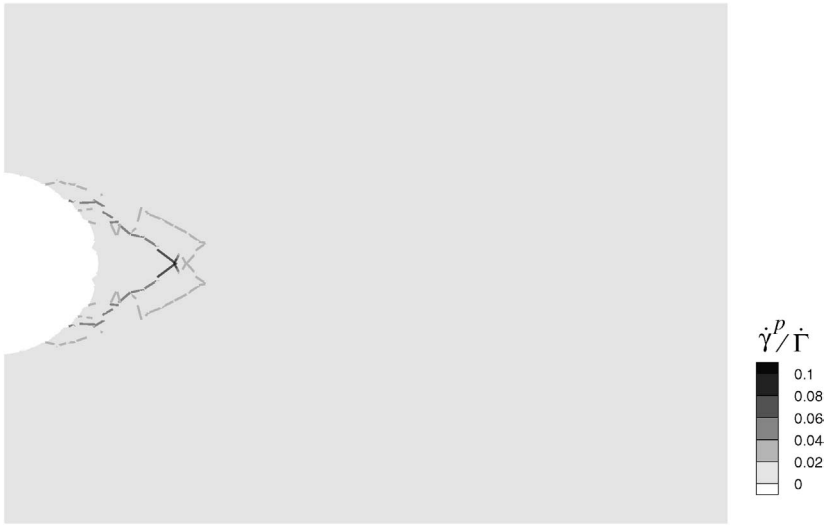

(a)

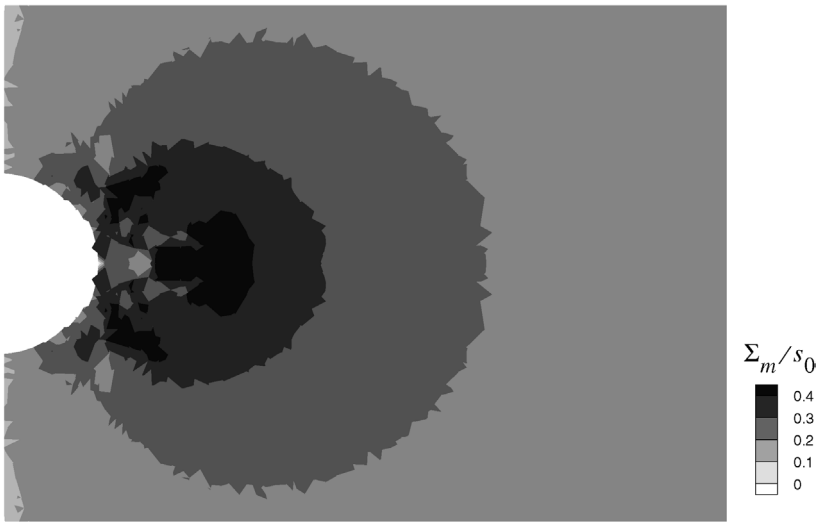

(b)

Fig. 11. (a) Plastic strain activity $\dot{\gamma}^p$ and cavitation zone at $\overline{K} = 1.2$; (b) Distribution of hydrostatic stress.

shear banding, respectively). To overcome these limitations a third modeling approach is adopted here by explicitly resolving a number of voids in the matrix around a crack tip in detail (Fig. 12). The matrix behavior is that of neat SAN as described in Section 2.1 while outside the voided region the homogenized continuum model of a porous polymer (Section 3) is employed. The void spacing relative to their size is determined by the rubber content which is taken to be $f_0 = 0.25$ in correspondence with the models in Sections 3 and 4. Treating a number of rubber particles close to the crack tip as voids from the beginning on can be motivated by the fact that the front of the cavitation zone depicted in Fig. 3 has already reached a considerable distance from the crack tip at the onset of yielding. As mentioned earlier, this model is quite expensive in view of the FE discretization required for the matrix, and the relative size-scale of voids and notch radius chosen here is not very realistic. It is, however, approximately the same as in the discrete shear surface model (Section 4). Essentially the model allows for both mechanisms investigated separately in the two previous sections and indeed, significant void growth as well as localized yielding in between individual voids can be seen in Fig. 12. Although the plastic zone extends only over a relatively small number of voids its elongated overall shape is akin that observed in experiments.

This agreement yet has to be taken with caution because the shape of the plastic zone in this model actually is sensitive to the local void arrangement. As illustrated in Fig. 13(a), positioning a single void (indicated by the arrow) by only less than a void radius closer to the notch (in an otherwise identical configuration as in Fig. 12) leads to a significantly different plastic

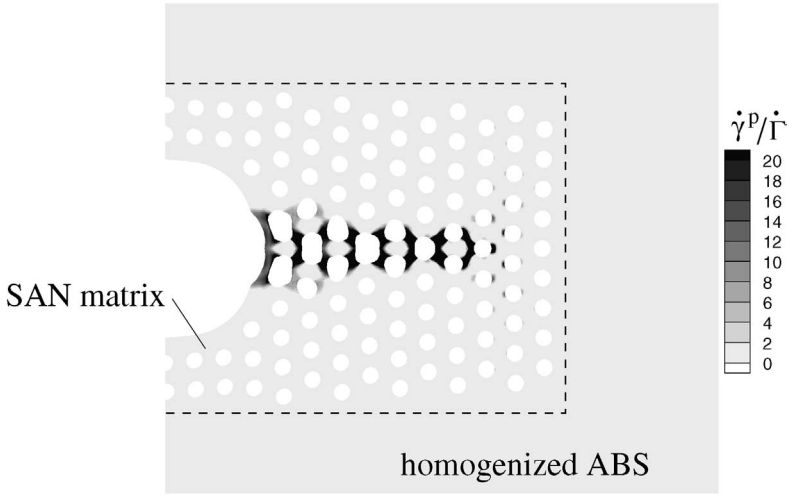

Fig. 12. Equivalent plastic strain rate at $\overline{K} = 1.2$ in region of explicitly modeled voids in SAN matrix surrounded by homogenized ABS.

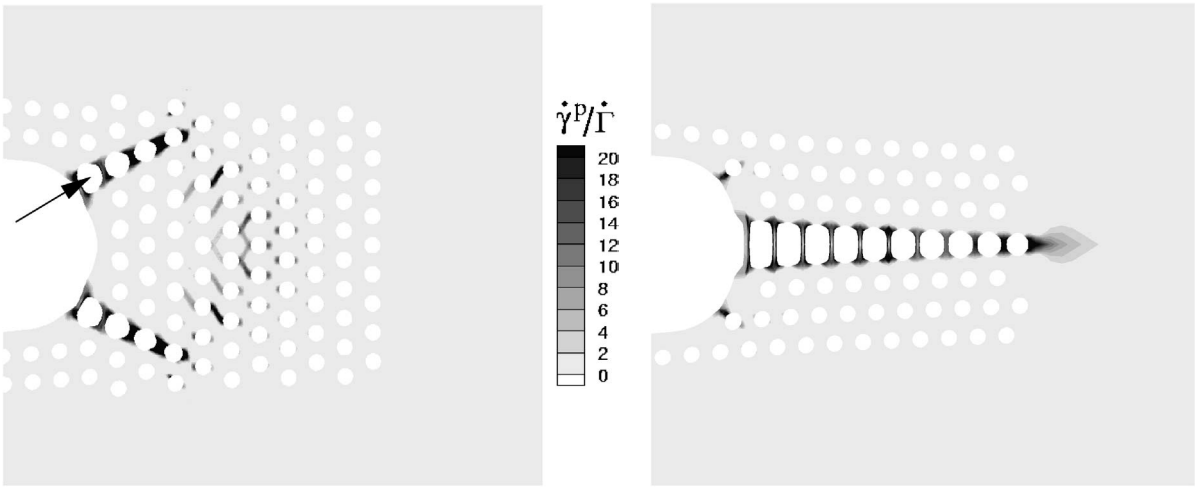

Fig. 13. Equivalent plastic strain rate at $\overline{K} = 1.2$ in region of explicitly modeled voids: (a) arrangement of Fig. 12 but with void indicated by arrow slightly shifted, (b) horizontal rows of voids with one row on ligament.

zone pattern. In the plastic zone of Fig. 13(a) the two deformation mechanisms focused on in the previous sections, i.e. intense void growth in a dilatational band and shearing between voids, appear clearly separated. Another example of the sensitivity of the plastic zone shape to the void arrangement is shown in Fig. 13(b) where the voids are located in horizontal rows and plastic deformation takes place solely by necking between the strongly growing voids of the center row ahead of the notch. To relax the critical issue of the dependence on local void arrangement somewhat, it should be mentioned that the localization of plasticity in very different patterns in the present cases is promoted by the regularity of the arrangement in vertical or horizontal rows of equal sized and equal spaced voids. In a random microstructure this problem is likely to be less severe.

While plastic zones in real ABS have a width comparable to the initial notch, Figs. 12 and 13 reveal that the tendency for localization in a much more narrow dilatational band found for the fully homogenized model (Fig. 3) is also present in the discrete void model. The strong dependence of the plastic zone on the actual void arrangement seen in the above examples to some extent results from the regularity of the arrangement in vertical or horizontal rows of equally sized and equally spaced voids. Furthermore, it may also be promoted by the present 2D modeling where the voids are in fact infinitely long cylinders favoring localization more than a 3D arrangements of ‘real’ voids (Socrate and Boyce, 2000). Hence, in a random 3D microstructure this problem might be less severe. In addition, a 3D model would provide more insight into the competition between void growth and shear banding which is likely to differ along the specimen thickness direction due the varying overall stress state.

Another simplification of the real material behavior may be the negligence of the load carrying capacity of the rubber directly upon cavitation or, as in the present model, from the beginning on; but, as discussed by Steenbrink and van der Giessen (1999), this depends on the rubber modulus.

6. Discussion and conclusion

We have presented various models to investigate inelastic deformations close to a crack tip in polymer-rubber blends. Special attention has been given to the ability of the models to reproduce characteristic features of the plastic zone at a crack tip. The plastic zone, which is the source of the superior toughness of these materials, results from local inelastic deformation mechanisms promoted by the preceding cavitation of the rubber particles. Two effects of rubber particle cavitation have to be distinguished: Firstly, particle cavitation enables the growth of voids rendering the whole material plastically dilatant and, secondly, it changes the matrix stress state to a more deviatoric one thus favoring local shear. The porous plasticity model (Section 3) and the shear surface model (Section 4) can be seen as complementary extreme cases, each emphasizing one of these effects. The porous plasticity model assumes the total amount of rubber (treated as voids) to contribute to plastic dilation via the overall yield function (6) and the associated flow rule (7). In contrast, the shear surface model is based on the assumption that the rubber particles essentially serve to promote shear banding in the matrix upon their cavitation and that their expansion (i.e. plastic void growth) can be neglected. While the spatial distribution of cavitation alone, taking place prior to plasticity, is equally well described by the two models, both have shortcomings in capturing the ensuing inelastic deformation mechanisms.

Void growth in the porous plasticity model introduces volumetric softening and localizes deformation in a zone which, though elongated as in real ABS, is unrealistically narrow. One reason for the overestimation of void growth may lie in the fact that an 'effective' post-yield hardening of the matrix phase, resulting from local molecular stretching in conjunction with the nonuniformity of plastic flow in real blends, is not properly accounted for in this homogenized material model.

The shear surface model, which works well under more deviatoric overall stress states (Pijnenburg and van der Giessen, 2003), in case of highly triaxial stress states suffers from the total neglect of void growth. Plastic deformation takes place in a rather diffuse zone which does not display the elongated shape known from experiments. Yet it resembles the shape obtained from the porous plasticity model when volumetric yield therein is likewise excluded. Hence, the elongated shape of the crack-tip plastic zone in real ABS seems to be tied to some amount of plastic dilatancy.

The explicit modeling of discrete voids in a plastically deformable matrix (Section 5) allows for all deformation mechanisms but becomes computationally too expensive when applied to realistic 3D microstructures. The 2D examples presented here, with a relatively small number of voids, suffer from the high sensitivity to the actual void arrangement. Therefore it is dangerous to extrapolate these results without critical assessment. Obviously this also applies for all other models introduced in this paper. However, in combination they provide valuable tools to investigate the relevant crack-tip plasticity mechanisms in greater detail. Moreover, they can serve as stepping stones to more advanced modeling.

In this regard it has to be mentioned that another mechanism, *crazing*, likewise important for inelastic deformation and energy dissipation in polymer-rubber blends, has been completely ignored in the present study. Models for distributed crazing in neat glassy polymers have been developed by Tijssens et al. (2000). Interestingly, when applied to the problem of a notch, the resulting zone of inelastic deformation also displays an elongated shape as investigated in the present work. It therefore appears not only necessary but also quite promising to incorporate distributed crazing in the modeling of rubber-toughened glassy polymers.

References

Arruda, E.M., Boyce, M.C., 1993. A three-dimensional constitutive model for the large stretch behavior of rubber elastic materials. J. Mech. Phys. Solids 41, 389–412.

Boyce, M.C., Parks, D.M., Argon, A.S., 1988. Large inelastic deformation of glassy polymers. Mech. Mater. 7, 15–33.

Bucknall, C.B., 1977. Toughened Plastics. Applied Science, London.

Chen, X.-H., Mai, Y.-W., 1999. Three-dimensional elastoplastic finite element modelling of deformation and fracture behaviour of rubber-modified polycarbonates at different triaxiality. J. Mat. Sci. 34, 2139–2149.

Danielsson, M., Parks, D.M., Boyce, M.C., 2002. Three-dimensional micromechanical modeling of voided polymeric materials. J. Mech. Phys. Solids 50, 351–379.

Donald, A.M., Kramer, E.J., 1982. Plastic deformation mechanisms in poly(acrylonitrile–butadiene styrene) [ABS]. J. Mat. Sci. 17, 1765–1772.

Gurson, A.L., 1977. Continuum theory of ductile rupture by void nucleation and growth. J. Engrg. Mat. Tech. 99, 2–15.

Ishikawa, M., 1995. Stability of plastic deformation and toughness of polycarbonate blended with poly(acrylonitrile–butadiene–styrene) copolymer. Polymer 36, 2203–2210.

Jar, P.-Y.B., Creagh, D.C., Konishi, K., Shinmura, T., 2002. Mechanical properties and deformation mechanisms in high thermal resistant poly(acrylonitrile–butadiene–styrene) under static tension and izod impact. J. Appl. Polym. Sci. 85, 17–24.

Jeong, H.-Y., Li, X.-W., Yee, A.F., Pan, J., 1994. Slip lines in front of a round notch tip in a pressure-sensitive material. Mech. Mater. 19, 29–38.
Lai, J., van der Giessen, E., 1997. A numerical study of crack-tip plasticity in glassy polymers. Mech. Mater. 25, 183–197.
Ni, B.Y., Li, J.C.M., Berry, V.K., 1991. Plastic zone in front of a mode I crack in acrylonitrile–butadiene–styrene polymers. Polymer 32, 2766–2770.
Pierce, D., Shih, C.F., Needleman, A., 1984. A tangent modulus method for rate dependent solids. Comp. Structures 18, 875–887.
Pijnenburg, K.G.W., Steenbrink, A.C., van der Giessen, E., 1999. Shearing of particles during crack growth in polymer blends. Polymer 40, 5761–5771.
Pijnenburg, K.G.W., van der Giessen, E., 2001. Macroscopic yield in cavitated polymer blends. Int. J. Solids Structures 38, 3575–3598.
Pijnenburg, K.G.W., van der Giessen, E., 2003. A novel approach to the analysis of distributed shear banding in polymer blends. Int. J. Numer. Meth. Engrg. 58, 703–721.
Ramaswamy, S., Lesser, A.J., 2002. Microscopic damage and macroscopic yield in acrylonitrile–butadiene styrene (ABS) resins tested under multi-axial stress states. Polymer 43, 3743–3752.
Seelig, Th., van der Giessen, E., 2002. Localized plastic deformation in ternary polymer blends. Int. J. Solids Structures 39, 3505–3522.
Smit, R.J.M., Brekelmans, W.A.M., Meijer, H.E.H., 1999. Prediction of the large-strain mechanical response of heterogeneous polymer systems: local and global deformation behavior of a representative volume element of voided polycarbonate. J. Mech. Phys. Solids 47, 201–221.
Socrate, S., Boyce, M.C., 2000. Micromechanics of toughened polycarbonate. J. Mech. Phys. Solids 48, 233–273.
Steenbrink, A.C., Gaymans, R.J., van der Giessen, E., 1994. The effect of strain rate and temperature on the deformation and fracture of ABS. In: Polymat '94. London, pp. 598–601.
Steenbrink, A.C., van der Giessen, E., 1997. Void growth in glassy polymers: effect of yield properties on hydrostatic expansion. Int. J. Damage Mech. 6, 317–330.
Steenbrink, A.C., van der Giessen, E., 1999. On cavitation, post-cavitation and yield in amorphous polymer-rubber blends. J. Mech. Phys. Solids 47, 843–876.
Steenbrink, A.C., van der Giessen, E., Wu, P.D., 1998. Studies on the growth of voids in amorphous glassy polymers. J. Mat. Sci. 33, 3163–3175.
Sue, H.-J., Yee, A.F., 1996. Micromechanical modeling of crack-tip rubber particle cavitation process in polymer toughening. Polym. Eng. Sci. 36, 2320–2326.
Tijssens, M.G.A., van der Giessen, E., Sluys, L.J., 2000. Modeling of crazing using a cohesive surface methodology. Mech. Mater. 32, 19–35.
Wu, P.D., van der Giessen, E., 1996. Computational aspects of localized deformations in amorphous glassy polymers. Eur. J. Mech. A Solids 15, 799–823.
Xu, X.-P., Needleman, A., 1994. Numerical simulation of fast crack growth in brittle solids. J. Mech. Phys. Solids 42, 1397–1434.